Particles II

Access the latest eBook →

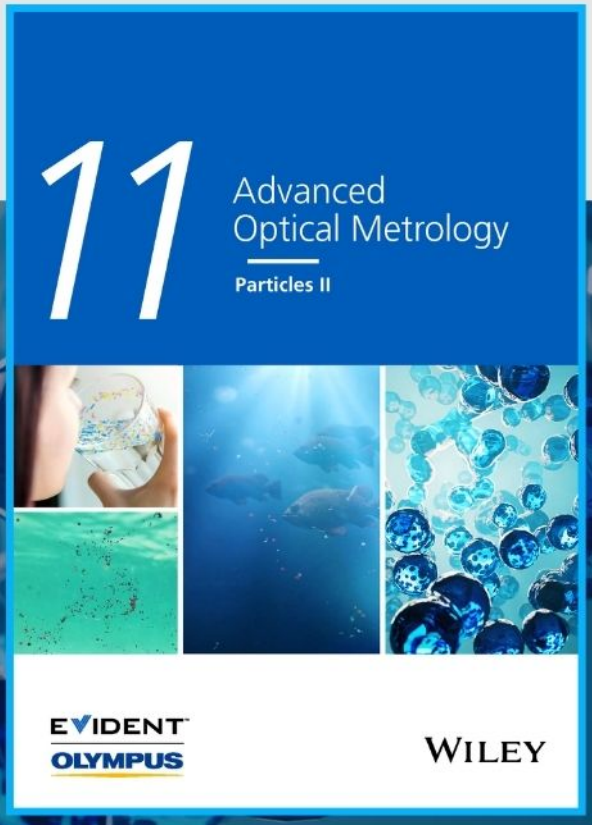

Impact on Biological Systems and the Environment

This eBook is dedicated to the research of Professor David Wertheim.
In collaboration with various groups, Professor Wertheim uses confocal microscopy to analyse the impact of different types of particles on human health and the environment, with a focus on human health-hazardous particles detected with solid-state nuclear track detectors (SSNTD). Download for free, today.

EVIDENT
OLYMPUS

WILEY

ADVANCED MATERIALS
www.advmat.de

A Wearable Supercapacitor Based on Conductive PEDOT:PSS-Coated Cloth and a Sweat Electrolyte

*Libu Manjakkal, Abhilash Pullanchiyodan, Nivasan Yogeswaran, Ensieh S. Hosseini, and Ravinder Dahiya**

A sweat-based flexible supercapacitor (SC) for self-powered smart textiles and wearable systems is presented. The developed SC uses sweat as the electrolyte and poly(3,4-ethylenedioxythiophene):poly(styrenesulfonate) (PEDOT:PSS) as the active electrode. With PEDOT:PSS coated onto cellulose/polyester cloth, the SC shows specific capacitance of 8.94 F g^{-1} (10 mF cm^{-2}) at 1 mV s^{-1}. With artificial sweat, the energy and power densities of the SC are 1.36 Wh kg^{-1} and 329.70 W kg^{-1}, respectively for 1.31 V and its specific capacitance is 5.65 F g^{-1}. With real human sweat the observed energy and power densities are 0.25 Wh kg^{-1}, and 30.62 W kg^{-1}, respectively. The SC performance is evaluated with different volumes of sweat (20, 50, and 100 µL), bending radii (10, 15, 20 mm), charging/discharging stability (4000 cycles), and washability. With successful on-body testing, the first demonstration of the suitability of a sweat-based SC for self-powered cloth-based sensors to monitor sweat salinity is presented. With attractive performance and the use of body fluids, the presented approach is a safe and sustainable route to meet the power requirements in wearable systems.

Wearable systems and smart textiles hold great potential for tackling pressing global challenges by providing solutions in the areas of healthy ageing, patient monitoring, emergency management, safety at work, productivity enhancement, energy management of homes, and self-health management, etc. Coupled with advances in the Internet of Things, virtual/augmented reality and robotics, the smart textile could also lead to a new level of human connectedness.[1] For these advances, the smart wearables should have high density of seamlessly integrated and self-powered active/passive devices (e.g., sensors, actuators, displays, and circuits for read out and communication).[2,3] As a result, there is growing interest in fibers-based devices, particularly for energy generation and storage to attain energy autonomous wearables.[2,3] Several attempts in this direction have focused on using conventional batteries, which restrict portability and wearability owing to issues such as nonflexibility, over-heating, use toxic electrolytes, and limited life span, etc. The flexible energy storage devices (e.g., batteries[4] and supercapacitors (SCs),[3,5] including those based on textiles, have been explored recently to address some of these issues and modest performances have also been demonstrated. However, like conventional energy storage devices, these energy storage devices have used toxic electrolytes, which pose safety risk when used in wearable systems and require special packaging to prevent electrolyte leakages.[6,7] These issues could be addressed with biocompatible materials and the unique work presented with in the first instance demonstrating the use of biofluids such as sweat for the development of flexible SC.

Sweat has been explored for energy generation using biofuel cells[8] and detection of chronic diseases through biosensors,[9–12] where the use of positive and negative ions from sweat constituents (e.g., Na^+, K^+, and Cl^-) are absorbed or diffused into surface of the working or sensitive electrode and thus take part in the electrochemical reaction. Here, we have considered such ionic reactions for electrochemical energy storage application. The major advantages of sweat for wearable SCs come from their nontoxicity, environmentally friendliness and as reliable electrolyte for wearable energy storage devices. This is in sharp contrast to the corrosive and flammable aqueous (acidic or alkaline) or organic electrolytes, which are widely used today. It may be noted that sweat equivalent based on NaCl, and KCl could also be used as electrolytes, but they are less attractive for wearable applications as additional storage arrangement will be needed for them and this may cause discomfort. On the other hand, sweat is readily available for wearables and can be extracted using iontophoresis techniques in needed.[10,12]

Herein, the developed SC uses a polyester cellulose cloth as substrate and the separator, and poly(3,4-ethylenedioxythiophene):poly(styrenesulfonate) (PEDOT:PSS) as both active electrode and current collector for sweat electrolyte. Due to the high absorption rate of cloth (due to natural cellulose fibers: 55% cellulose and 45% polyester), the body sweat is quickly

Dr. L. Manjakkal, Dr. A. Pullanchiyodan, Dr. N. Yogeswaran, Dr. E. S. Hosseini, Prof. R. Dahiya
Bendable Electronics and Sensing Technologies (BEST) Group
School of Engineering
University of Glasgow
Glasgow G12 8QQ, UK
E-mail: Ravinder.Dahiya@glasgow.ac.uk

The ORCID identification number(s) for the author(s) of this article can be found under https://doi.org/10.1002/adma.201907254.

DOI: 10.1002/adma.201907254

absorbed and as a result, the developed SC shows appreciable performance even with very low amount of sweat (20 µL). As compared to traditional electrolytes, the concentration of ions in sweat is low (e.g., Na^+ is (66 ± 46) × 10^{-3} M and K^+ is (9 ± 4.8) × 10^{-3} M)[10] and in this regard highly active material such as PEDOT:PSS is attractive as it offers both mixed ionic and electronic conductivity, better bonding with textiles, low temperature processing, and good biocompatibility. In fact the use of PEDOT:PSS as a sensitive electrode for body-fluid-based electrochemical sensors has been successfully demonstrated.[11,13] Further, the high specific capacity of PEDOT:PSS-based SC (which also depends on the electrolytes, e.g., 103 F g^{-1} in 1 M Et_4NBF_4/acetonitrile[14] and 130 F g^{-1} in 1 M H_2SO_4[15]), the high conductivity (10^{-2} to 10^3 S cm^{-1}),[16] large voltage window (1–1.5 V),[16,17] flexibility/bendability, environmental friendliness, cost effectiveness, etc., make the PEDOT:PSS an excellent electrode for SC fabrication.[18] A comparison of various PEDOT:PSS-based SCs is given in Table S1 of the Supporting Information. Even though PEDOT:PSS has been widely reported for SC fabrication, in the case of textile-based SCs it is normally deposited on the top of carbon fibers and commonly uses the toxic acidic electrolytes such as H_3PO_4 and H_2SO_4 (Table S1, Supporting Information). Instead, we are reporting here for the first time the use of PEDOT:PSS as a single electrode (both as current collector and an active electrode). The SC electrodes are fabricated by simple low-cost drop casting method. To enhance the conductivity, the PEDOT:PSS was doped with dimethyl sulfoxide (DMSO).[19,20] Adhesion between the PEDOT:PSS with polyester fabric and cellulose fibers has been studied separately in previous works reported in the literature.[21] Here, the stable adhesion between PEDOT:PSS and cellulose/polyester cloth is due to the strong electrostatic and hydrogen bonding interactions of the charged PEDOT:PSS and the hydroxyl groups of cellulose. Owing to the presence of natural cellulose fibers, the cloths offer excellent wet absorption capacity for the PEDOT:PSS ink.[22] These features of PEDOT:PSS led to appreciable improvement in the electrochemical performance of the presented SC. The redox reaction of PEDOT:PSS conjugated polymer film and the formation of high electrochemical double layer capacitance (EDLC) at the electrode–electrolyte interface, as shown in **Figure 1**, have also contributed to improved performance. The schematic of the fabricated symmetric SC with cross-section of the electrodes is shown in Figure S1a of the Supporting Information. Here, a plain cellulose/polyester cloth was wrapped around the electrode to enhance absorption of the forming sweat and thereby the performance of SCs.[6,23] The fabricated SC shows specific capacitance of 8.94 F.g^{-1} (10 mF cm^{-2}) at 1 mV s^{-1} for 0.8 V in sweat equivalent electrolyte and is comparable with reported values (Table S1, Supporting Information). Thus, the presented flexible SC act as a distinct energy storage device for energy autonomous smart wearables. This is also demonstrated here by powering a textile-based chemiresistive sensor with energy stored in the sweat-based SC to monitor the sweat salinity.

The textile-based electrodes for the SC are fabricated by drop casting method and is shown in **Figure 2**a. The optical photograph of the cloth before and after coating with PEDOT:PSS are shown in Figure 2b,c. Due to the uneven and rough surface of the cloth (Figure 2b), the drop casting technique was adopted here as an easy method to coating ink onto the substrate. The change in the surface morphology of the cloth after drop casting of the PEDOT:PSS on cellulose fabric was analyzed using scanning electron microscopy (SEM) images

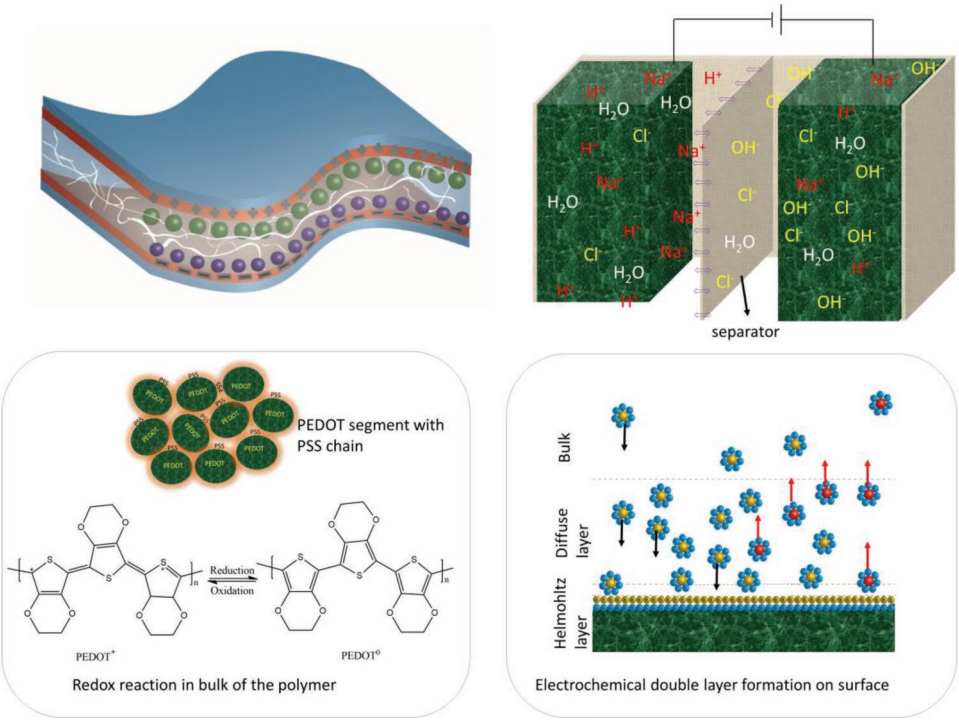

Figure 1. Schematic representation and mechanism of the PEDOT:PSS coated on cellulose cloth, which absorbs sweat as an electrolyte for wearable supercapacitors.

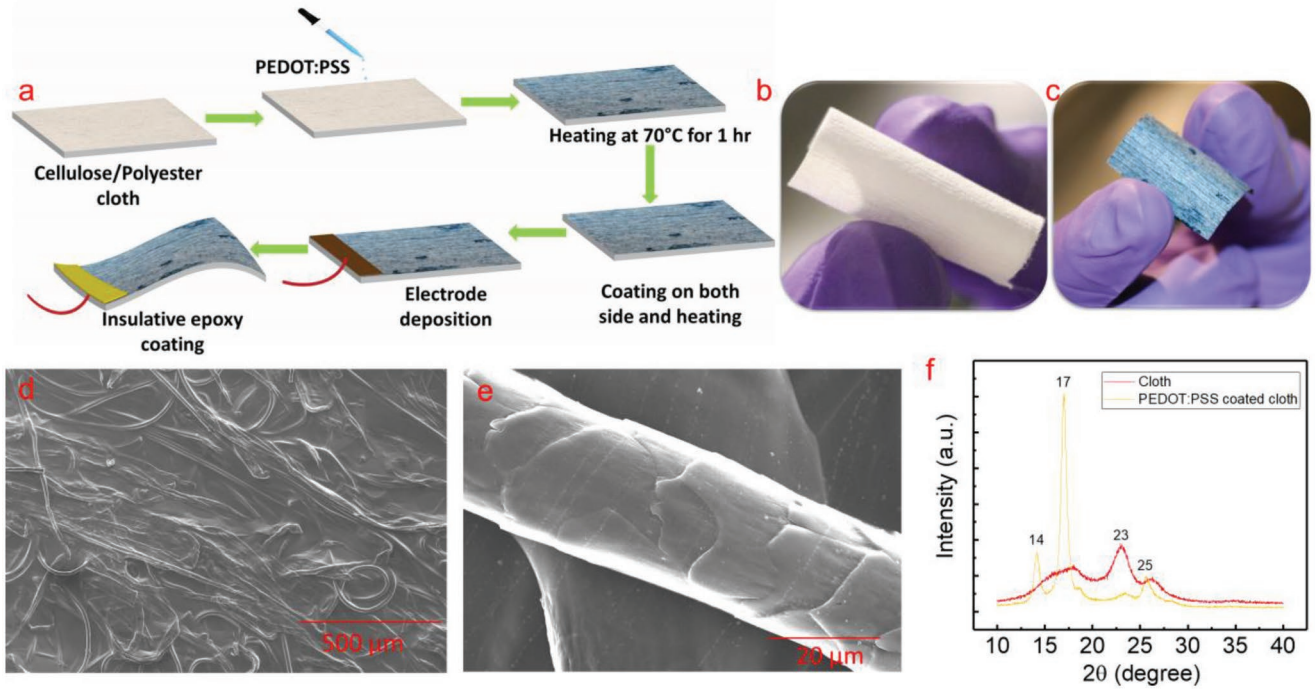

Figure 2. Fabrication mechanism and characterization of the textile SC and electrodes. a) Scheme for the fabrication of PEDOT:PSS-based electrodes on cloth. b,c) Photographs of the cloth before and after PEDOT:PSS coating. d,e) SEM images of the cloth after PEDOT:PSS coating with an enlarged view of a single thread. f) Comparison of XRD spectrum of the cloth and PEDOT:PSS doped with DMSO-coated cloth.

(Figure 2d,e). SEM image of the cloth before coating is given in Figure S1b,c of the Supporting Information. The PEDOT:PSS-coated film on the cloth was observed as uneven surface shown in SEM (Figure 2e). The magnified images in Figure 2e shows that each fiber of the cloth is well coated with PEDOT:PSS.

The X-ray diffraction (XRD) pattern, of the PEDOT:PSS-coated cloth is shown in Figure 2f. The comparison of XRD patterns for pure cloth and PEDOT:PSS-coated cloth (in Figure 2f) shows the interchain stacking crystalline formation of the film with sharp peaks at 14°, 17°, and 25.6°. For PEDOT:PSS-coated fabric, the XRD peak at $2\theta = 25.6°$ (corresponds to the lattice spacing of 3.5 Å) should be attributed to the distance between π–π stacking of the PEDOT chains and confirms the formation of PEDOT:PSS phase on the surface of the cloth.[24] As reported earlier, PEDOT:PSS characteristic peaks appeared at 17.5° and 25.8°.[25] The addition of DMSO solvent causes a sharper peaks of the PEDOT:PSS nanofibers, which observed at 17° and the peak at 14° could be related to excess of PSS in the film.[26] Further, the conductivity (0.14 S cm^{-1}) of the electrode was calculated from *IV* measurements (plot shown in Figure S1d, Supporting Information). We observed that PEDOT:PSS with DMSO electrode showed an enhanced conductivity in comparison with PEDOT:PSS electrode (0.05 S cm^{-1}). Figure S1e of the Supporting Information shows the electrical characterization of PEDOT:PSS doped with DMSO and the PEDOT:PSS film (in inset) coated on a glass slide. It was found that the PEDOT:PSS film exhibited a higher resistance in comparison to the PEDOT:PSS with DMSO. Further, as evident from the *IV* measurements (Figure S1d,e, Supporting Information), both PEDOT:PSS and PEDOT:PSS DMSO coated on cloth exhibited a higher resistance in comparison to film on glass slide. This could be attributed to the high contact resistance and the rougher cloth surface. We observed that as compared to pure PEDOT:PSS, the DMSO added PEDOT:PSS coated in glass has almost three orders of magnitude higher conductivity. The optical image of glowing the red LED (Figure S1f, Supporting Information) shows the conductivity of the fiber after integrating with the circuit.

The electrochemical properties of the SC including the ion exchange, charge-transfer, equivalent series resistance (ESR), and the capacitance were investigated by electrochemical impedance spectroscopic (EIS) analysis in the frequency range of 10 mHz to 10 kHz. The Nyquist plot for fabric SC in sweat electrolyte is shown in **Figure 3**a. In the low frequency range, the impedance decreases sharply with increasing frequency and a horizontal plateau is observed at high frequencies (shown in the inset of Figure 3a). The straight line (not vertical) in the low frequency range of Nyquist plot (Figure 3a) shows the slower diffusion of the ions into the electrode and the capacitive behavior of PEDOT:PSS-based SC. The low impedance value (less than 300 Ω at 10 mHz for the imaginary part of the complex impedance) represent the good access of the sweat ion to the PEDOT:PSS electrodes. The absence of semicircle in the high frequency range in Nyquist plots or the smaller value of charge transfer resistance (R_{ct}) exhibit the high conductivity of the electrode during reaction with sweat electrolytes. Hence, we observed a negligible bulk resistance of electrode and the ESR was observed at the high frequency intercept (10 kHz) of the Z_{real} in Nyquist plot. The fabricated PEDOT:PSS exhibits comparable or less ESR value, 6.3 Ω (1.26 Ω cm^{-2}) with respect to the state-of-the-art PEDOT:PSS and other materials based SCs.[27,28] For example, the 6.3 Ω of DMSO-doped

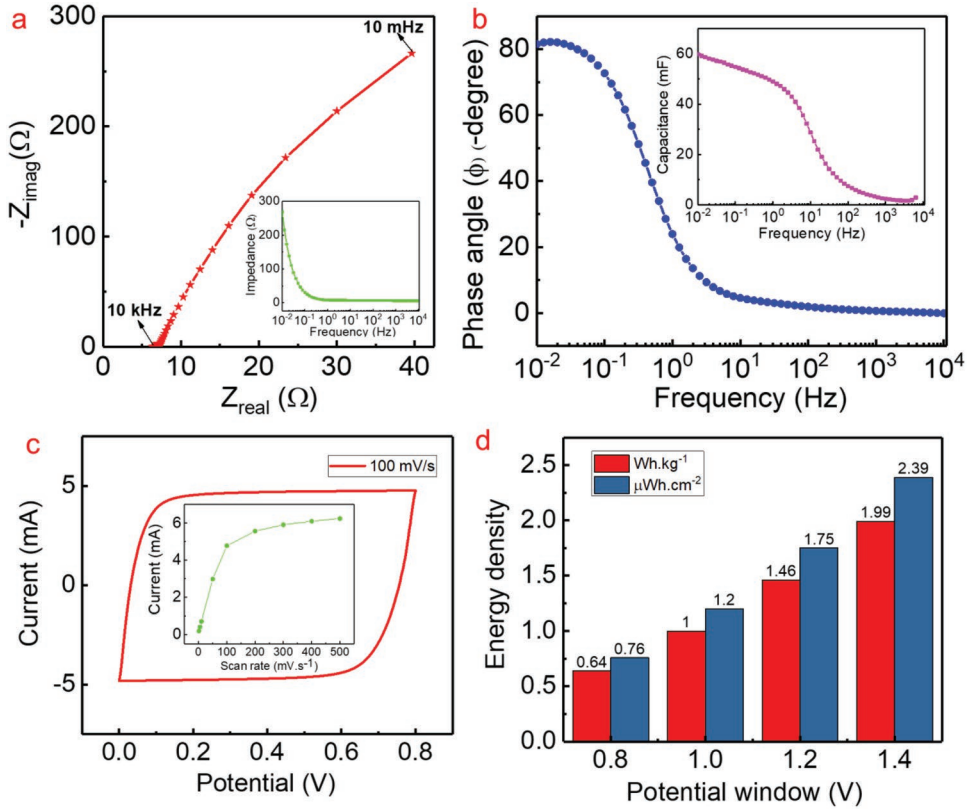

Figure 3. Electrochemical (EIS and CV) analysis of the SC. a) Nyquist plot for SC in sweat solution (inset shows impedance variation with frequency) in the frequency range of 10 mHz to 10 kHz. b) Bode phase angle plot for the SC in sweat electrolytes (variation of capacitance with frequencies shown in inset). c) PEDOT:PSS SC at a scanning rate of 100 mV s^{-1} and inset shows the peak current versus scan rate. d) The variation of the energy density of the SC with increasing potential windows.

PEDOT:PSS by spray coating method[27] and 7.3 Ω cm^{-2} for aramid nanofibers/PEDOT:PSS (ANFs/PEDOT:PSS) in PVA/H_2SO_4 gel electrolyte.[28] The low value of ESR and R_{ct} of the SC also implies the sweat ions having good pore accessibility to the fiber electrode during electrochemical reaction.[29] The relaxation time constant (τ_0), which represents the dielectric relaxation characteristic of the whole system,[30] of the device was measured (2.5 s) from the characteristic frequency (f_0) (i.e., the frequency at −45° phase angle where the capacitive and resistive impedances are equal) by using the expression $\tau_0 = 1/f_0$. Further, the relaxation time constant of the SC was found to be 2.5 s and it represent the minimum time needed to discharge all the energy (high power delivery) with an efficiency of more than 50%.[31,32]

From the Bode phase angle plot in Figure 3b, we observed that in low frequency region, the phase angle (−82°) is closer to the ideal capacitor value (i.e., −90°). The Bode plot analysis reveals ideal capacitive performance of textile PEDOT:PSS-based SC in sweat solution. The capacitance with variation of frequency was measured by using the expression reported in previous works using imaginary component of the complex impedance data.[30,33] The capacitance of SC for varying frequencies is shown inset of Figure 3b. The measurement reveals that PEDOT:PSS-coated-cloth-based SC with sweat electrolyte shows capacitance of 59 mF (capacitance density of 9.8 F g^{-1}) at a frequency of 10 mHz. The high capacitance 9.8 F g^{-1} in the low frequency range is due to the intercalation (ions diffusion to the pores of the electrode) of sweat–electrode interface. Due to the redox reaction in the conjugated polymers and the high conductivity of the electrode, both pseudocapacitance and electrochemical double layer (EDL) formation occur on the surface of PEDOT:PSS electrode, as shown in Figure 1. It is believed that due to the two-phase structure of PEDOT:PSS film (hole-conducting PEDOT- and ion-conducting PSS grains), the contribution to the total capacitance is also partly contributed during the electrochemical reaction between these phases.[34] The etching process of PSS film by DMSO to enhance the conductivity of PEDOT:PSS film, results in the formation of porous structure of PSS film. This facilitates the access of ions in the electrolyte to get into the inner grains of the polymer, as shown in Figure 1 and Figure S1a (Supporting Information), resulting in the formation of the EDL.[20,34] In addition, the leftover DMSO solvent in PEDOT:PSS film induces a screening effect between the positively charged PEDOT and negatively charged PSS chain, which reduce the coulomb interaction between them and facilitate redox reaction.[35] Cations from the sweat electrolyte (Na^+ or K^+) enter the PEDOT:PSS channel and the oxidized $PEDOT^+$ can be reduced to its natural state by ions exchange with the sweat electrolyte, as per the following reaction (also shown in Figure 1)

$$PEDOT^+:PSS^- + M^+ (\text{from sweat}) + e^- \leftrightarrow PEDOT^0 + M^+:PSS^- \quad (1)$$

Cyclic voltammetry (CV) analyses were carried at different scan rate in the range of 1 to 500 mV s^{-1} for a potential window of 0.8 V. Figure 3c shows the CV curve of the SC at scan rate of 100 mV s^{-1} at 0.8 V. In high scan rates a more rectangular shape in CV curve observed as compared to low scan as shown in Figure S2a (for 1 mV s^{-1}) of the Supporting Information. Figure S2b of the Supporting Information shows CV curves for wide scan rate (1–500 mV s^{-1}). The increasing scan rate results in higher peak current, as shown in Figure 3c for a voltage of 0.8 V. As suggested by previous reports, CV measurement for symmetric PEDOT:PSS electrode configuration shows that oxidation occurs in one electrode and reduction in the other.[36] In our measurement with sweat electrolyte, we did not observe strong redox peaks in low or high scan rates (Figure 3c). The quasi-rectangular shape of the CV curve in low scan rate denotes the redox reaction in the conjugated polymer and such shape is normal in pseudocapacitance due to the redox reaction of the conductive polymers.[37] In low scan rate, almost all ions from the sweat electrolyte diffuse into the pores of the electrode and contribute to the pseudocapacitance by utilizing all active sites of the fiber conductive electrode. However, at high scan rate the CV curve maintains rectangular shapes, indicating the fast charging–discharging properties of the device with high power density. The high scan rate measurement also predicts the capacitive behavior of the device which is similar to double layer-based SC with fast ionic diffusion.[38] As confirmed by the diffusion of ions into the pores of the electrode, Figure 3c in CV analysis depicted an almost linear behavior between lower scanning rate and current. We observed that, the redox peaks also depend on the type of electrolyte. To confirm this, we also tested by using H_3PO_4 as an electrolyte of this fabric SC. In low scan rate (Figure S3a, Supporting Information) redox peaks and in high scan rate rectangular shape of CV curve were observed (shown in Figure S3b, Supporting Information).

In addition to the capacitance value, the maximum energy storage of the devices also depends on the operating potential window. In order to maximize potential window, CV analyses were carried out for different potential windows (0.8, 1, 1.2, and 1.4 V) at a scan rate of 100 mV s^{-1}. The result, shown in Figure S2c of the Supporting Information, indicates that at high voltage the spike in the rectangular CV curve increases with increasing of potential window. This is due to the voltage drop (IR_{drop}) of the SC.[31] A detailed investigation of the IR_{drop} is discussed below.

The specific capacitance (C_{sp}) was measured in terms of weight (F g^{-1}) (weight of electrodes 0.006 g) and area (mF cm^{-2}) (area of the device 5 cm^2) by using Equation (S1) of the Supporting Information. Here we observed that for sweat electrolyte, at low scan rate (1 mV s^{-1}) the C_{sp} of the SC is 8.94 F g^{-1} (10 mF cm^{-2}) and for high scan rate (500 mV s^{-1}) it is 1.84 F g^{-1} (2.21 mF cm^{-2}). This observation of decreasing C_{sp} with increasing scan rate is similar to one reported in the literature.[39] A substantial decrease in the specific capacitance (from 8.9 F g^{-1} for 1 mV s^{-1} to 1.84 F g^{-1} for 500 mV s^{-1}) with increase in scan rate was observed. This is because during high scan rate the ions from the sweat electrolyte (Na^+ or K^+) only reach on the outer surface of the fiber electrode instead of diffusing into the pores of the fiber electrode, which is observed during the low scan rate.[40] This reduces the number of active sites participating in the reaction and hence intercalation capacitance of the electrode during the high scan rate. The increase in the potential window also results in a slight variation in the maximum attained C_{sp}. The comparison (in weight and area) of the observed C_{sp} for different potential windows at 100 mV s^{-1} is shown in Figure S2d of the Supporting Information. For instance, at a potential window of 1.4 V the maximum C_{sp} is 8.8 F g^{-1} in comparison to 8.6 F g^{-1} for 0.8 V potential window. A slight increase in specific capacitance with increase in the voltage window for a fixed scan rate was observed for the SC with maintaining of almost same rectangular shapes.

The energy density (E) with respect to weight and area was measured by using Equation (S2) of the Supporting Information. From CV analysis at a scan rate of 1 mV s^{-1}, the energy density was found to be 0.80 Wh kg^{-1} (0.90 μWh cm^{-2}). We observed that the energy density decreases (at 0.8 V potential window) with increasing scan rate. The energy density of the SC at 500 mV s^{-1} is 0.16 Wh kg^{-1}. As energy density is proportional to the square of voltage (from Equation (S2), Supporting Information), it was found that the energy density increased with higher voltage window, as shown in Figure 3d at 100 mV s^{-1}. The device shows high energy density of 1.99 Wh kg^{-1} (2.39 μWh cm^{-2}) at 1.4 V than the energy density of 0.64 Wh kg^{-1} (0.76 μWh cm^{-2}) at 0.8 V at scan rate of 100 mV s^{-1}. The high operating voltage performances with excellent CV curves indicate the fast charging–discharging properties of the device with high energy and power density.

The sweat concentrations can vary considerably with health conditions, daily activities, and between individuals. To investigate the influence of such variations, we carried out a detailed analysis by testing the SC with varying concentration of NaCl from 0×10^{-3} to 180×10^{-3} M and KCl from 0×10^{-3} to 12×10^{-3} M in the sweat equivalent electrolyte. We observed (Figure S4a, Supporting Information) that the increase in NaCl concentration tends to increase the conductivity of the electrolyte. The CV curve of the SC in sweat electrolyte under these conditions is shown in **Figure 4**a. Except slight variation in the area under the curve and the peak current, the CV is almost similar at different NaCl concentrations. We calculated the pNa (–log [Na^+]) and plotted it against peak current, as shown in Figure 4b. For higher concentrations of Na^+ (180×10^{-3} M), the maximum peak current is 4.5 mA. Slight increase in the peak current can be noted with higher concentrations of Na^+. This leads to a minor variation in the capacitance at low NaCl concentrations. The relative change in capacitance (without and with NaCl) is 4%, as shown in Figure 4c. For higher concentrations of NaCl or conductivity of the sweat electrolyte, the maximum relative change in capacitance is 11%, as shown in Figure 4c. We also measured the EIS of the SC at different NaCl concentrations. From the Nyquist plot (Figure S4b, Supporting Information), we observed that the diffusion resistance decreases in the low frequency and the ESR value decreases in the high frequency. This is due to the presence of high ionic constituents and the conductivity of the electrolyte. Similar studies carried out with KCl (0×10^{-3} to 12×10^{-3} M concentration) showed minor changes as may be noted from the CV and Nyquist plots in Figure S4c,d of the Supporting Information.

The galvanostatic constant current charging and discharging (GCD) measurements of the fabricated SC in sweat electrolyte

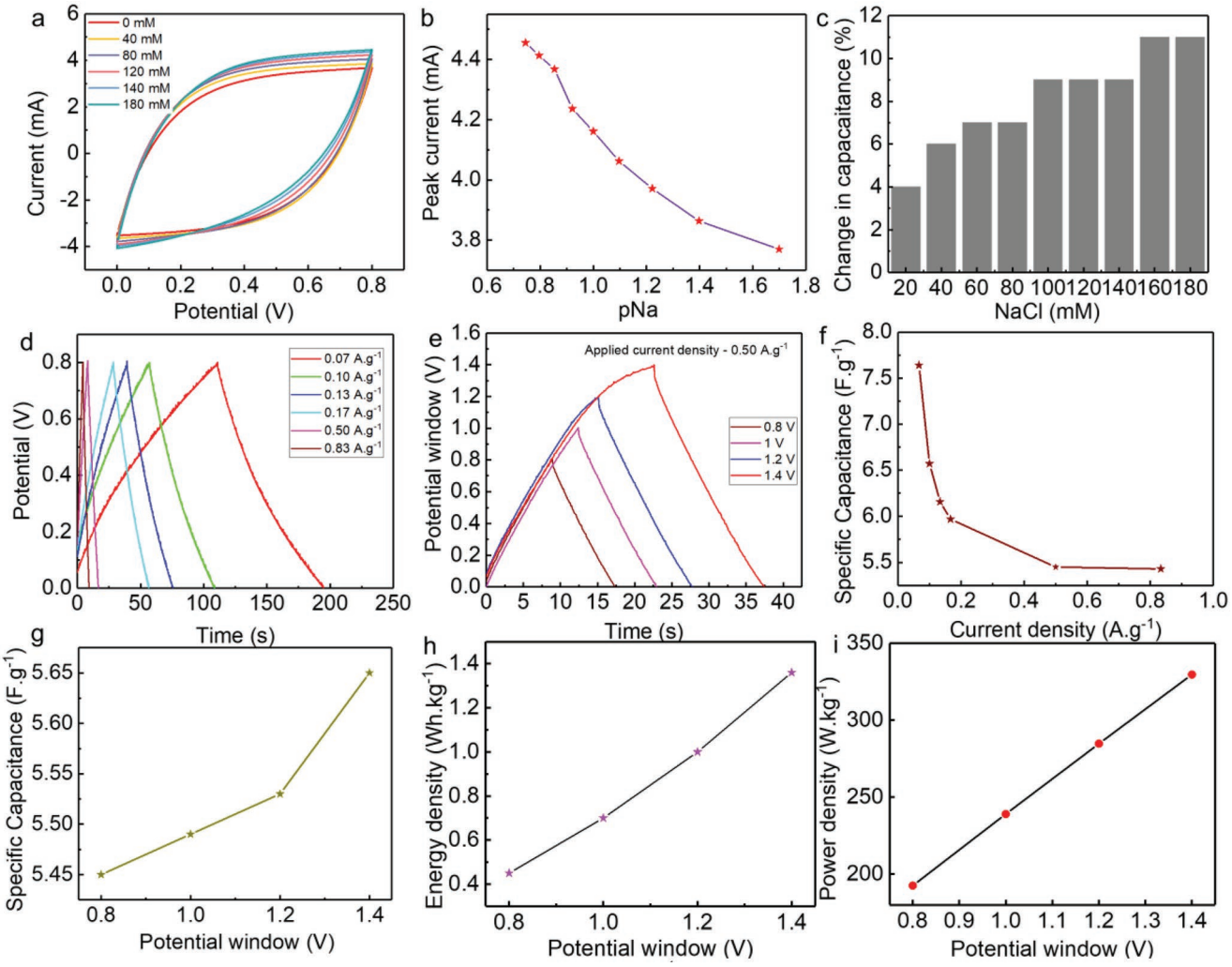

Figure 4. a) CV analysis of the SC at 100 mV s^{-1} for different concentration of NaCl in the sweat electrolyte. b) The variation of peak current with pNa of the electrolyte. c) Relative capacitance changes with NaCl concentration in the sweat electrolyte of the SC. d) GCD for different current densities at a potential window of 0.8 V. e) GCD measurement for different potential windows at fixed applied current density of 0.50 A g^{-1}. f,g) Variation of specific capacitance in terms of weight for different current density and potential window. h,i) The variation of energy and power density (inset) for different potential windows.

at 0.8 V window are compared in Figure 4d for current densities ranging from 0.07 to 0.83 A g^{-1}. The dependence of GCD on potential window (in the range of 0.8 to 1.4 V) was measured by applying a current density of 0.5 A g^{-1}, as shown in Figure 4b. The triangle-shaped GCD curves indicate the EDLC behavior of the SC and are confirmed by the CV and EIS analysis also. The symmetrical shapes GCD curves in Figure 4d,e indicate a high reversibility of the fabricated PEDOT:PSS electrode in sweat electrolyte during the charging/discharging processes in a wide current densities and potential windows. It was found that the IR_{drop} changes with increasing applied current or potential window. This variation is shown in Figure S5a,b of the Supporting Information. For GCD measurement in the potential window of 0.8 V, the IR_{drop} of 7 and 80 mV was observed at a low (0.07 A g^{-1}) and high (0.83 A g^{-1}) current densities, respectively. For a current density of 0.5 A g^{-1}, the IR_{drop} for the potential window of 0.8 V is around 30 mV and this increases to 81 mV for 1.4 V window. The very low voltage drop (7 mV) at current density of 0.07 A g^{-1} indicates lower internal resistance of the material and hence the excellent power characteristic of the device in sweat electrolyte. The ESR value of the SC could be calculated from the IR_{drop} (ESR is obtained by dividing the IR_{drop} with by twice the applied current)[33] and for low applied current the value ESR found to be 1.75 Ω cm^{-2} and is almost equal to the value (1.26 Ω cm^{-2}) observed from EIS analysis (Nyquist plot). Even though the material has very low internal resistance, we observed an increase in the IR_{drop} with increase of current density and the voltage window in GCD measurement (Figure S5a,b, Supporting Information). This could be due to the electrolyte potential drop. Similar performance was observed for the conducting polymer-based SC.[41] In majority of aqueous electrolyte-based SCs, the operating voltages are limited to 1.3 V due to the water decomposition.[42] We observed that, after IR compensation, the device shows operating voltage of 1.31 V and hence at high-voltage window the potential drop in electrolyte is due to the decomposition of water. Hence, from

the above analysis in this work we found that the *IR* drop of the sweat-based SC depends on the internal resistance, voltage window, electrolyte potential drop, and applied current density.

We measured the C_{sp}, energy density and power density from GCD measurements by considering the IR_{drop} using Equations (S3) to (S5) of the Supporting Information. Figure 4f,g shows the C_{sp} in terms of mass for different current densities and the potential windows. The SC shows highest C_{sp} of 7.64 F g^{-1} (8.45 mF cm^{-2}) at the low current density of 0.07 A g^{-1} and the C_{sp} value decreases with increasing the current density, as evident from Figure 4f and Figure S5c (Supporting Information). Like CV measurement, the C_{sp} value increases slightly with increasing potential window (Figure 4g). The energy and power density of SC were obtained by using the C_{sp} and the potential window of 0.8 V. The energy and power densities are 0.61 Wh kg^{-1} (0.74 μWh cm^{-2}) and 26.20 W kg^{-1} (0.031 mW cm^{-2}) respectively for a current density of 0.07 A g^{-1}. It was observed that with increase in the current density results a decrease in energy density but increase of power density, as shown in Figure S5d,e and Ragone plot in Figure S5f of the Supporting Information. The energy and power density measurements were also carried out for the different potential windows and it was found that the energy and power densities increase with increasing the potential window, as shown in Figure 4h,i. The observed high energy density was 1.36 Wh kg^{-1} (1.63 μWh cm^{-2}) at 1.31 V (after considering the IR_{drop} at 1.4 V and its C_{sp} 5.65 F g^{-1} at a current density of 0.5 A g^{-1}) potential window and the power density was 329.70 W kg^{-1} (0.40 mW cm^{-2}).

From energy and power densities measurements we found that they generally increase with the increase in the operating potential window. However, for fixed potential window (0.8 V) the energy density decreases, and power density increases as the current densities becomes higher. In majority of reported PEDOT:PSS based SCs, the high energy densities were obtained by using metal oxide or carbon-based PEDOT:PSS composites as an active electrode with ionic gel or aqueous acidic or basic electrolytes.[43,44] Here in this work, the measured energy density 1.36 Wh kg^{-1} (1.63 μWh cm^{-2}) and power density 329.70 W kg^{-1} (0.40 mW cm^{-2}) of the SC is comparable with the PEDOT:PSS based on different electrolytes, for example, the energy density of the PEDOT:PSS with aluminum solid electrolytic (0.16 Wh kg^{-1}),[45] RuO_2/PEDOT:PSS hybrid thin films with H_2SO_4/PVA gel electrolyte (0.053 μWh cm^{-2}, 147 μW cm^{-2}),[44] PEDOT:PSS/AgNFs with H_2SO_4/PVA (0.09 μWh cm^{-2} at a power density of 0.93 μW cm^{-2})[46] and others as shown in Table S1 of the Supporting Information.

Further, the detailed electrochemical properties of the SC were evaluated with cyclic charging and discharging for 4000 cycles at a potential window of 0.8 V (Figure S6, Supporting Information). **Figure 5**a depicts the electrochemical performance of SC with GCD, EIS, and CV measurements: i) after initial cycle; ii) after 4000 cycles; iii) drop casting of artificial sweat after 4000 cycles. In stage (i) the freshly prepared SC electrode contained high volume of electrolyte. The investigations about stability during cyclic charging/discharging over 4000 cycles shows a variation in electrochemical performance due to the lack of electrode–electrolyte interaction and material degradation, as evident from the Nyquist plots in stage (i), stage (ii), and stage (iii) of Figure 5a. This could be attributed to the evaporation of the water in the sweat electrolyte due to local heating[28] after 30 h of continuous measurements. Moreover, in comparison to the initial cycle, after long charging–discharging, the electrode surface got degraded (shown in SEM image after electrochemical reaction in Figure S7, Supporting Information) due to electrochemical reaction resulting in the observed variation in the shape of the CV curve in stage (ii) and stage (iii) as compared to stage (i). Further, the device shows Coulombic efficiency of 93.11%, IR_{drop} of 18 mV, C_{SP} of 6.631 F g^{-1} (from GCD measurement) and ESR 6.3 Ω. After 4000 cycles, stage (ii), the SC shows almost same Coulombic efficiency (from charging–discharging analysis), but lower charging and discharging time compared to stage (i). In stage (ii) the IR_{drop} increased to 63 mV, C_{sp} decreased to 4.93 F g^{-1}, and ESR increased to 195 Ω. As compared to rectangular shape of CV curve of stage (i), a quasi-rectangular CV curve is observed in stage (ii) for the scanning rate of 100 mV s^{-1}. The CV analysis shows capacitive retention of about 75% after 4000 cycles. The energy density of the device measured from the first cycle is 0.59 Wh kg^{-1} and after 4000 cycles is 0.44 Wh kg^{-1}. The CV analysis shows the energy density of the device after 4000 cycles due to the retention in the capacitance. Further analysis was carried out in stage (iii), where we drop casted sweat electrolyte onto the SC electrodes after 4000 cycles. One of the advantages of the fabricated SC is that it regains the performance to a greater extent after dropping the sweat (electrolyte), but with low capacitive/energy storage capability as compared to fresh sample. From stage (iii) it was observed that the Coulombic efficiency of the SC suddenly decreased to 46.7% and IR_{drop} increased to 71 mV. In stage (iii) the contact resistance and the ESR value were decreased as compared to step (ii) but still it is three times higher in comparison to stage (i). CV curve shows a similar trend of step (ii). This shows that even when the sweat is present, the SC performance varies due to electrode degradation after 4000 cycles. We also evaluated the long charging/discharging performances at 1.3 V of operating potential for about 5000 cycles, as shown in Figure S8 of the Supporting Information. The initial 10 and final 10 cycles are shown as magnified images in Figure S8a of the Supporting Information. By comparing the first and last cycle, it can be concluded that the fabricated SCs show a sharp potential drop from 0.22 to 0.79 V and show the capacitive retention of the device. We measured the capacitive retention and observed around 87% for 1000 cycles and around 70% for 2000 cycles (shown in Figure S8, Supporting Information). We found that the capacitive retention of the SC reached around 45% after 5000 cycles due to high IR_{drop} of the device and lack of the electrolytes.

Further studies were carried out to investigate the influence of the volume of sweat (20, 50, and 100 μL) on the SC performance. For this study, a miniaturized SC was fabricated (0.5×2 cm^2 and the total weight of the electrodes is 0.0038 g) as shown in Figure S9a,b of the Supporting Information. Figure 5b shows the variation of CV curve under different volumes of sweat. At low volume (20 μL), the SC exhibited a weak performance. The detailed EIS and CV analyses were carried out and are presented in Figure S10 of the Supporting Information. The performance of SC under different volume of sweat is summarized in the table of Figure 5b.

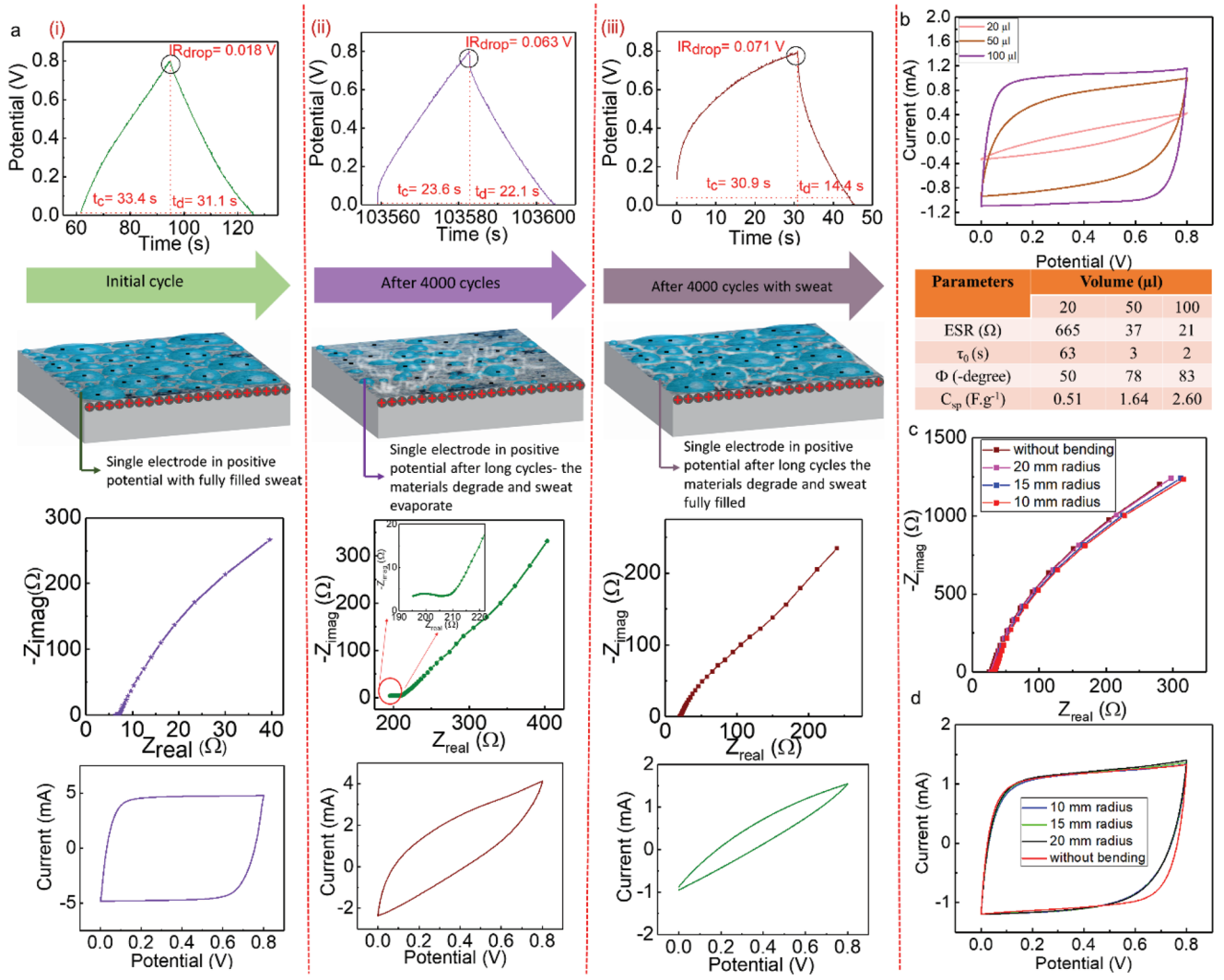

Parameters	Volume (µl)		
	20	50	100
ESR (Ω)	665	37	21
τ_0 (s)	63	3	2
Φ (-degree)	50	78	83
C_{sp} (F.g^{-1})	0.51	1.64	2.60

Figure 5. Electrochemical performance of SC in various conditions. a) Cyclic stability in presence of sweat (i): initial cycle of the GCD, EIS and CV analysis and schematic of single electrode under positive potential with sweat. (ii) GCD, EIS, and CV analysis after 4000 charging/discharging cycles and the schematic of single electrode under positive potential, the sweat evaporated and materials degraded. (iii) GCD, EIS, and CV analysis of SC after 4000 cycles, but again enriched with sweat, and the schematic of single electrode under positive potential. b) CV measurements of SC under different volume of sweat and performance table. c,d) Nyquist and CV plots of SC under different bending conditions.

The higher volume of electrolyte (100 µL) of sweat resulted in an improved performance thereby signifying the importance of the electrolyte volume in SC. In low volume of sweat, the active sites involved in the electrochemical reaction are lesser and there are fewer ions involved in the intercalation. A quasi-rectangular CV curve was observed for 20 µL electrolyte as compared to rectangular CV curve for 100 µL volume of electrolyte, Figure S10 (iii) of the Supporting Information. At lower sweat amount (less than 50 µL), and after the long cycle performance, the high ESR value (Figure S10 (i), Supporting Information) shows the surface degradation of material and the lack of ions available for the reaction. Further, we measured SC performance under different bending radius 10, 15, and 20 mm, respectively (Figure S9b, Supporting Information). No noticeable change in the performance of SCs was observed with bending as illustrated in Figure 5c,d through Nyquist plot and CV curve.

For practical applications, the cyclic bending of the device is needed. The GCD measurements were carried out at 1000 cycles of bending with radius of 25 mm. This much bending may be expected in wearable applications. Figure S11 and Movie S1 of the Supporting Information show the GCD curves during the cyclic bending. Figure S11a of the Supporting Information shows the image of bending setup and Figure S11b of the Supporting Information shows the GCD curve with magnified curve for first and last cycle. The measurements (the first and the last cycle of GCD curve during cyclic bending shown in Figure S11c,d, Supporting Information) of GCD reveal that the discharge time and IR_{drop} of the SC is almost same during the cyclic bending of the device.

In addition to the bending and cyclic stability measurement, we also measured the performance of SC after washing. The CV analysis before and after washing (Figure S12a, Supporting Information) at scan rate of 100 mV s^{-1} shows that after

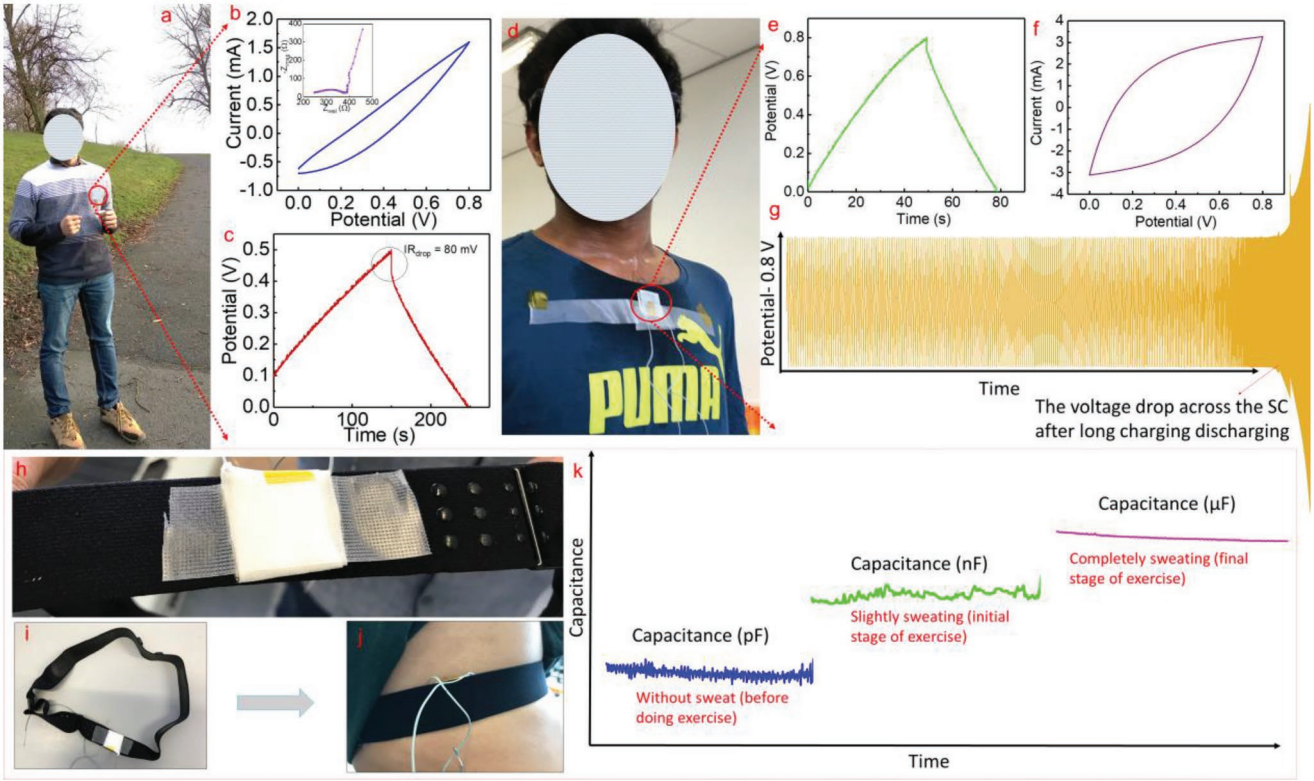

Figure 6. Performance of the sweat-based SC in real application. a) Image of the person with partly wet (due to sweat) SC attached to clothes. b) The CV (inset EIS) and c) GCD analysis of the partly wet SC with human sweat as an electrolyte. d) The image of fully wet (due to sweat) SC attached on cloth. e,f) GCD and CV analysis of the fully wet SC. h–j) The textile SC on a polar pro strap for conformal contact and k) the energy storage capability of SC with increasing the amount of sweat during exercise.

washing a quasi-rectangular CV curve is observed and is similar to the analysis which we found after material degradation in Figure 5. This material degradation is confirmed from the EIS analysis in Figure S12b of the Supporting Information. The ESR value of material is increased after washing (7 Ω before washing and 22 Ω after washing) and it could be due to loss of some materials during washing.

Sweating may vary from person to person, daily activity, and the physiological status of individuals. In this work, we carried out the performance of the textile SC in different sweating and exercise conditions for two persons. Initially, we attached the SC into cloth and device is partially wetted (image is shown in **Figure 6**a) by real human sweat during running in a park. The electrochemical analysis of the SC with real human sweat as the electrolyte, shown in Figure 6b, CV (inset shows EIS) and Figure 6c, GCD. The SC with real human sweat exhibited a poor performance in comparison to SC with a 20 μL artificial sweat. This is due to the low amount of sweat, which is insufficient to wet the cloth completely. It was observed that the SC (with real human sweat as an electrolyte) showed a high ESR value (≈240 Ω) and charge transfer resistance (≈140 Ω) and the CV is looks similar to the device with low volume of sweat equivalent (Figure S10 (iii), Supporting Information). In low volume of sweat, there are insufficient ions for reaction, which leads to high charge transfer resistance and the ESR value. The performance of SC analyzed from GCD measurements showed a high IR_{drop} (80 mV). The measured energy and power densities are 0.095 Wh kg^{-1} and 3.81 W kg^{-1}, respectively, at a low current density of 0.016 A g^{-1}. In order to confirm the influence of sweat volume (wetting) on device performance, we carried out a detailed studies for high volume of sweat with different exercise conditions. The SC attached to the shirt (Figure 6d) was fully wet while running on treadmill (see Video S2, Supporting Information) when the electrochemical performance was evaluated. The Nyquist plot shown in Figure S13a of the Supporting Information reveals low ESR value (≈40 Ω) and negligible charge transfer resistance as compared with partially wetted device. The GCD curve for the SC during running is shown in Figure 6e. The SC shows an excellent charging/discharging performance at a potential of 0.8 V (IR_{drop} is 60 mV) and high current density of 0.085 A g^{-1} as compared to partly wetted device (0.016 A g^{-1}). The measured energy and power densities are 0.25 Wh kg^{-1}, and 30.62 W kg^{-1}, respectively, at a low current density of 0.085 A g^{-1}. As compared to Figure 6b, the CV curve for the device, fully wetted with sweat (Figure 6f), shows high area under the curve in a potential window of 0.8 V at 100 mV s^{-1}. The CV analysis for partially wetted SC (person 1) at 100 mV s^{-1} shows C_{sp} of 2.08 F g^{-1}, which is much lower than 7.06 F g^{-1} for fully sweat wetted SC (person 2). The observed specific capacitance at 100 mV s^{-1} is similar to the one from sweat equivalent solution (7.18 F g^{-1}, shown in Figure 3h). The stability of capacitance with and without sweating is shown in Figure S13b of the Supporting Information (measured by using LCR meter at 100 Hz). The long charging/discharging

GCD performances of fully wetted SC, analyzed at room temperature for 0.8 V at 0.5 mA current, is shown in Figure 6g. It was observed that the SC voltage drops after 950 cycles, at that point due to the evaporation of sweat the electrodes become dry and the SC stopped working. As compared to the first cycle, when it is fully wet with sweat (GCD is shown in Figure S13c, Supporting Information), the GCD at 950th cycle shows high drift in potential during charging/discharging. These results are shown in Figure S13d of the Supporting Information.

In order to increase the wettability, we also attached the textile SC with polar pro strap (Polar H10) to allow the conformal contact of SC with the body during fitness test and exercise (shown in Figure 6h–k) (see Video S3, Supporting Information). We evaluated the energy storage capability of SC during sweating (person 1). Without any sweating (i.e., start of exercise), the SC shows capacitance in pF range. As soon as sweating starts, the capacitance increases to nF range and finally reached the µF range with full sweating (Figure 6k). These results show the performances of SC under various exercise stages and sweating conditions.

Compared with other PEDOT:PSS based SCs (with nonsweat-based electrolytes) reported in the literature[44,46,47] (Ragone plot in **Figure 7**a), we found that the developed biocompatible SC shows excellent performance. It was observed that the device shows excellent performance even with very low amount sweat and can power wearable sensors in such conditions. Finally, as a proof of concept the fabricated SC was integrated with textile-based saline sensor for sweat monitoring applications. The low voltage (15 mV) required for the operation of chemiresistive saline sensor (due to the conductive nature of the sensitive electrode) can be supplied by the presented SC. The performance of the sensor with schematic of the measurement is shown in Figure 7b. The intention of this study is to demonstrate the potential of fabricated SC for self-powered wearables/textiles. New 3D schematics and image of the hybrid structure of the self-powered system are shown in Figure 7c. For the fabrication of the self-powered system, a single textile SC module and a salinity sensor were placed underneath of an amorphous silicon (a-Si) flexible photovoltaic cell (Sanyo, AT7665A 664-6841) (PV). The results shown in Figure S14 of the Supporting Information

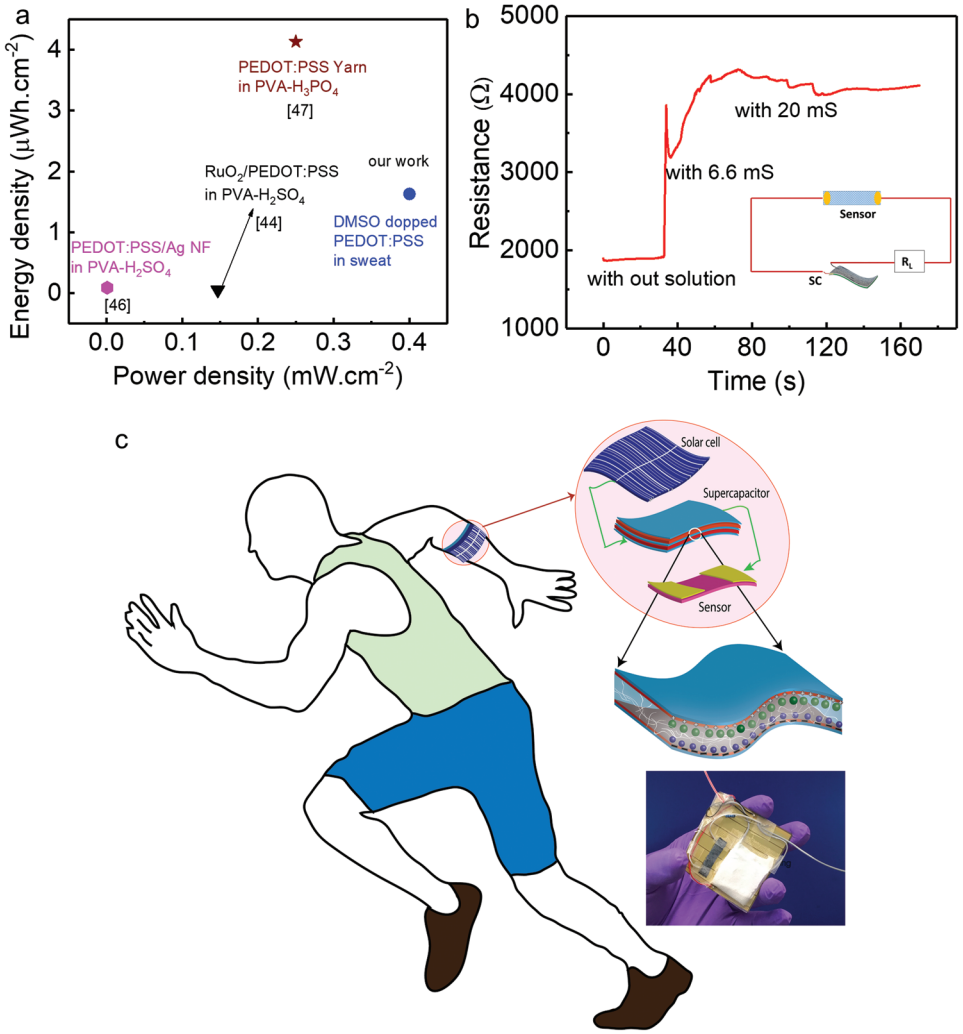

Figure 7. a) Ragone plot showing comparison of PEDOT:PSS SC performance. b) The SC powering a chemiresistive sensor (schematic in inset) for sweat salinity monitoring. c) Schematic of self-powered power pack and image in bottom.

indicate that the arrangement is sufficient for energy autonomous operation of wearable sensors. The charging/discharging of the SC with and without the PV cell is shown in Figure S14d of the Supporting Information. When the SC was charged by using solar cell, a sharp increase in potential was observed in Figure S14d of the Supporting Information. After charging, the solar cell was disconnected, and the stored potential is shown in Figure S14d of the Supporting Information. For initial testing we integrated the energy pack (solar cell and the SC) to the chemiresistive sensor and the observed variation in resistance is shown in Figure S14e of the Supporting Information. We observed that, with real human sweat (fully wetting condition), the observed energy and power densities are 0.25 Wh kg^{-1} and 30.62 W kg^{-1} (0.036 mW cm^{-2}), respectively. This demonstrates that the textile SC with sweat electrolyte is a viable solution for self-powered wearable system having sensors that require low power (nW cm^{-2}).

The major concerns regarding the cloth-based SC with sweat as an electrolyte are the material degradation, the fast evaporation of sweat from the cloth and the low capacitance as compared to PEDOT:PSS-based composite electrode and ionic or traditional electrolyte-based SCs. To overcome these issues we further carried two studies, as proof of-concept: i) using Ecoflex-based partial package to prevent the degradation of PEDOT:PSS electrode, and ii) printing new graphite: CuO composite on the top of PEDOT:PSS to enhance the performance. To reduce the evaporation of absorbed electrolyte and prevent material degradation, we coated a thin layer of Ecoflex on one side of the (exposed area) electrode, leaving behind a small active area as uncoated. As mentioned earlier, the cellulose cloth used in the SC offers high absorption capacity and hence by capillary action ensures the distribution of electrolyte on the cloth even if the active area of the coated electrode is wetted by the electrolyte (shown in Figure S15a, Supporting Information). The electrochemical analysis of the polymer-coated electrode-based SC shows a performance comparable with the noncoated electrode-based SC (Nyquist plot and GCD analysis are shown in Figure S15c,d, Supporting Information). Hence, this approach suggests a new way to improve the performance of the device without affecting its architecture. In addition, through the printing of graphite–CuO paste on the top of PEDOT:PSS-coated cloth, we also carried out preliminary studies to enhance the capacitance of sweat-based SC. As like PEDOT:PSS, due to better electrochemical activity, suitable surface charge, tuneable surface structure, and excellent ionic conductivity the CuO is widely used for biosensors, SCs, etc.[48] However, due to low electric conductivity the CuO composite finds limited use as electrode for SCs. This issue is overcome in this paper with new composite of CuO with graphite. Here, graphite provides the conductive path for CuO and is bonded with the PEDOT:PSS by the binder in the paste. The SEM and energy-dispersive X-ray spectroscopy (EDX) images of the printed electrode on top of cellulose cloth, presented in Figure S16a,b of the Supporting Information, show a good CuO nanoparticle distribution on the graphite network. With pseudocapacitive behavior of CuO and electrochemical double layer formation of graphite, the electrode offers excellent performance, which is confirmed by the electrochemical analysis (Figure S16c–f, Supporting Information). The Nyquist plot in Figure S16c of the Supporting Information shows the low value of impedance for the ion exchange. As compared to the diffusion of ions in low frequency (for PEDOT:PSS), here we observed the adsorption of ions (exhibited from the large arc in low frequency). The variation of capacitance with frequency in Figure S16d of the Supporting Information reveals the capacitance of 250 mF at low frequency (1 mHz). Further, the CV analysis shows that at 1 mV s^{-1} the SC has capacitance of 27.8 mF cm^{-2}, which is almost three times higher than PEDOT:PSS-coated-cloth-based SC (10 mF cm^{-2}) using sweat equivalent electrolyte. This study reveals the new area of investigation of materials for high energy density wearable energy storage devices using body fluid-based electrolyte.

As a future step, in addition to new materials (e.g., liquid metals which are stretchable, highly electrically conductive, stretchable, soft, and skin compatible),[49] a detailed analysis with power management circuit will be needed along with the energy storage device such as the one presented here.[23] There are several areas which need further improvements for practical applications of the fabricated SC. For example, the constituents of sweat, including NaCl, glucose, urea, Na_2SO_4, $NaHCO_3$, KCl, NaCl, $MgCl_2 \cdot 6H_2O$, NaH_2PO_4, $CaCO_3$, NH_4OH, etc. may vary from person to person and the physiological status of individuals. Further studies about the ionic or analytes concentration levels in real sweat on the performance of the SC will be carried out in the next work. Similarly, washability and long-term stability studies of the device will improve its practical applications.

In conclusion, in this work we present a textile-based supercapacitor using sweat as an electrolyte. The developed SC comprises a DMSO-doped PEDOT:PSS-coated cloth as an active electrode and sweat as an electrolyte. Due to both pseudocapacitance of conjugated polymers (Faradaic reaction) and electrochemical double layer formation occurring on the surface of PEDOT:PSS electrode when reacting with sweat, the fabricated SC gives an excellent performance. The developed sweat-based SC shows high specific capacitance for both artificial sweat (7.64 F g^{-1} in terms of weight and 8.45 mF cm^{-2} in terms of area at the low current density, 0.07 A g^{-1}) and the real human sweat (3.88 F g^{-1}). For an artificial sweat the device shows an energy density of 1.36 Wh kg^{-1} (1.63 μWh cm^{-2}) and power density of 329.70 W kg^{-1} (0.40 mW cm^{-2}) for 1.31 V (after considering the IR_{drop} at 1.4 V and its C_{sp} 5.65 F g^{-1}). With real human sweat the observed energy and power densities are 0.25 Wh kg^{-1}, and 30.62 W kg^{-1}, respectively. In this work the sweat is used as a monitoring parameter for health as well as a fuel for the energy storage device. The current studies provide the novel fabrication and implementation of the SC in wearable applications including its usage as a power source for the sweat monitoring sensors.

Experimental Section

Preparation of Solution and SC: For this work, PEDOT:PSS purchased from Ossila, UK (PH 1000) and DMSO was purchased from Sigma-Aldrich. For the electrode fabrication the PEDOT:PSS was mixed with 5 wt% of DMSO for 30 min using magnetic stirring, then it was drop casted on the cloth and dried at 85 °C for 1 h. As compared to pure PEDOT:PSS, the PEDOT:PSS dissolved in DMSO shows excellent electrochemical performance due to the increased conductivity of the material (as shown

in Figure S17, Supporting Information). Here the SC performance based on PEDOT:PSS dissolved in DMSO has been extensively studied. Artificial sweat was prepared by using the reported method[10] which involve 0.5 wt% of NaCl (Sigma-Aldrich), 0.1 wt% of KCl (Sigma-Aldrich), 0.1 wt% of lactic acid (Sigma-Aldrich), and 0.1 wt% of urea (Sigma-Aldrich) in deionized water and the pH adjusted to 6.5 ± 0.05 by dropwise addition of 0.1 M NaOH (Sigma-Aldrich), 0.1 M lactic acid (Sigma-Aldrich). The positive and negative ions from sweat constituents such as Na^+, Cl^-, K^+, Cl^-, lactic acid, urea, etc. take part in the electrochemical reaction. A digital pH meter (HI 98130 from Hanna Instruments) was used to measure the pH value of sweat. A polyester/cellulose blend fabric (Techni Cloth, TX612) was used as a substrate and separator.

Characterization: The surface morphology of PEDOT:PSS films was observed from SEM and EDX images (Hitachi SU8240, 15 kV and working distance (WD) of 8 mm). The crystalline structure of the PEDOT:PSS film was carried out using X-ray diffractometer (XRD), (P'Analytical X'Pert, with Cu Kα (λ = 1.514 Å)). The conductivity of the film was measured by *IV* plot. The electrochemical and supercapacitive performances of the SCs such as CV and EIS were evaluated using Metrohm Autolab (PGSTAT302N, The Netherlands) electrochemical workstation. The CV analysis of the SC was carried out at a scan rate of 1–500 mV s^{-1} in a potential range of 0 to 1.4 V. The EIS measurements of the symmetric SC in two electrode systems configurations were carried out from 10 mHz to 10 kHz at sinusoidal signals of 10 mV. The GCD measurements of the fabricated SCs were tested by using source meter (Agilent, U2722A) controlled with LabVIEW program at different current densities with a potential window 0 to 1.4 V. The GCD measurements were carried out for 1000 bending cycles with up to 25 mm bending radius. For sensor application, the chemiresistive sensor was fabricated on cloth by depositing PEDOT:PSS. The salinity of artificial sweat solution varied by adding diluted NaCl into the distilled water. For measurement a similar approach, reported in the previous work, was followed.[23] The conductivity of the solution was measured by using commercial digital meter (HI 98130 from Hanna Instruments).

Sweating may vary from person to person, exercise condition, and the physiological status of individuals. Detailed studies were carried out with high volume of sweat generated with different exercise conditions. The SC attached to the shirt was fully wet while running on treadmill (see Videos S2 and S3, Supporting Information) when the electrochemical performances were evaluated.

For further improvement, as a proof of concept, an active electrode for the SC was prepared by mixing graphite (Sigma-Aldrich) with CuO nanoparticle having particle size of 100 nm (Sigma-Aldrich). Graphite–CuO powder was prepared in the ratio of (1:0.5) wt% by mechanically mixing. Graphite–CuO mixture was used for thick film paste and prepared by thoroughly mixing the powder with 40 wt% of ethyl cellulose as a binder and terpinol as a solvent in an agate mortar. The printed paste on the top of PEDOT:PSS-coated cloth was heat treated at 80 °C for 1 h in an oven. The SEM and EDX images of graphite:CuO film were analyzed.

Supporting Information

Supporting Information is available from the Wiley Online Library or from the author.

Acknowledgements

This work was supported in part by the EPSRC through Engineering Fellowship for Growth (EP/M002527/1 and EP/R029644/1) and Royal Society-SERB Newton International Fellowship (NIF\R1\182437). The authors are thankful to James Watt Nanofabrication Centre (JWNC) and Electronic Systems Design Centre (ESDC) at University of Glasgow for support related to fabrication and characterization of the prototype devices. The authors are thankful to Prof. Jason Gill and his team for allowing the use of the treadmill and other lab facilities for the validation of SC. The sweat in the real demonstration was generated by normal running in open space and treadmill in the lab. The volunteers involved in the running exercise are also the co-authors of this manuscript. No ethical approval was required in this case.

Conflict of Interest

The authors declare no conflict of interest.

Keywords

energy materials, PEDOT:PSS, smart textiles, supercapacitor, sweat, wearable

Received: November 5, 2019
Revised: November 28, 2019
Published online: May 11, 2020

[1] a) R. Dahiya, *Proc. IEEE* **2019**, *107*, 247; b) C. G. Núñez, W. T. Navaraj, E. O. Polat, R. Dahiya, *Adv. Funct. Mater.* **2017**, *27*, 1606287; c) L. Capineri, *Proc. Eng.* **2014**, *87*, 724; d) R. Dahiya, N. Yogeswaran, F. Liu, L. Manjakkal, E. Burdet, V. Hayward, H. Jörntell, *Proc. IEEE* **2019**, *107*, 2016; e) R. Dahiya, D. Akinwande, J. S. Chang, *Proc. IEEE* **2019**, *107*, 2011.
[2] C. García Núñez, L. Manjakkal, R. Dahiya, *npj Flexible Electron.* **2019**, *3*, 1.
[3] J. S. Heo, J. Eom, Y. H. Kim, S. K. Park, *Small* **2018**, *14*, 1703034.
[4] a) S. Pang, Y. Gao, S. Choi, *Adv. Energy Mater.* **2018**, *8*, 1702261; b) Y.-H. Lee, J.-S. Kim, J. Noh, I. Lee, H. J. Kim, S. Choi, J. Seo, S. Jeon, T.-S. Kim, J.-Y. Lee, J. W. Choi, *Nano Lett.* **2013**, *13*, 5753.
[5] a) M. Liu, Z. Cong, X. Pu, W. Guo, T. Liu, M. Li, Y. Zhang, W. Hu, Z. L. Wang, *Adv. Funct. Mater.* **2019**, *29*, 1806298; b) Y. Huang, H. Hu, Y. Huang, M. Zhu, W. Meng, C. Liu, Z. Pei, C. Hao, Z. Wang, C. Zhi, *ACS Nano* **2015**, *9*, 4766.
[6] L. Manjakkal, W. T. Navaraj, C. G. Núñez, R. Dahiya, *Adv. Sci.* **2019**, *6*, 1802251.
[7] S.-Y. Lee, K.-H. Choi, W.-S. Choi, Y. H. Kwon, H.-R. Jung, H.-C. Shin, J. Y. Kim, *Energy Environ. Sci.* **2013**, *6*, 2414.
[8] a) A. J. Bandodkar, J.-M. You, N.-H. Kim, Y. Gu, R. Kumar, A. M. V. Mohan, J. Kurniawan, S. Imani, T. Nakagawa, B. Parish, M. Parthasarathy, P. P. Mercier, S. Xu, J. Wang, *Energy Environ. Sci.* **2017**, *10*, 1581; b) J. Lv, I. Jeerapan, F. Tehrani, L. Yin, C. A. Silva-Lopez, J.-H. Jang, D. Joshuia, R. Shah, Y. Liang, L. Xie, F. Soto, C. Chen, E. Karshalev, C. Kong, Z. Yang, J. Wang, *Energy Environ. Sci.* **2018**, *11*, 3431.
[9] H. Y. Y. Nyein, W. Gao, Z. Shahpar, S. Emaminejad, S. Challa, K. Chen, H. M. Fahad, L.-C. Tai, H. Ota, R. W. Davis, *ACS Nano* **2016**, *10*, 7216.
[10] W. Dang, L. Manjakkal, W. T. Navaraj, L. Lorenzelli, V. Vinciguerra, R. Dahiya, *Biosens. Bioelectron.* **2018**, *107*, 192.
[11] W. Gao, S. Emaminejad, H. Y. Y. Nyein, S. Challa, K. Chen, A. Peck, H. M. Fahad, H. Ota, H. Shiraki, D. Kiriya, D.-H. Lien, G. A. Brooks, R. W. Davis, A. Javey, *Nature* **2016**, *529*, 509.
[12] S. Emaminejad, W. Gao, E. Wu, Z. A. Davies, H. Yin Yin Nyein, S. Challa, S. P. Ryan, H. M. Fahad, K. Chen, Z. Shahpar, S. Talebi, C. Milla, A. Javey, R. W. Davis, *Proc. Natl. Acad. Sci. USA* **2017**, *114*, 4625.
[13] a) S. Nakata, T. Arie, S. Akita, K. Takei, *ACS Sens.* **2017**, *2*, 443; b) G. Tarabella, M. Villani, D. Calestani, R. Mosca, S. Iannotta, A. Zappettini, N. Coppedè, *J. Mater. Chem.* **2012**, *22*, 23830.
[14] D. Villers, D. Jobin, C. Soucy, D. Cossement, R. Chahine, L. Breau, D. Bélanger, *J. Electrochem. Soc.* **2003**, *150*, A747.

[15] K. Liu, Z. Hu, R. Xue, J. Zhang, J. Zhu, *J. Power Sources* **2008**, *179*, 858.
[16] K. Sun, S. Zhang, P. Li, Y. Xia, X. Zhang, D. Du, F. H. Isikgor, J. Ouyang, *J. Mater. Sci.: Mater. Electron.* **2015**, *26*, 4438.
[17] Z. Zhao, G. F. Richardson, Q. Meng, S. Zhu, H.-C. Kuan, J. Ma, *Nanotechnology* **2016**, *27*, 042001.
[18] L. V. Kayser, D. J. Lipomi, *Adv. Mater.* **2019**, *31*, 1806133.
[19] a) S. Kirchmeyer, K. Reuter, *J. Mater. Chem.* **2005**, *15*, 2077; b) G. H. Kim, L. Shao, K. Zhang, K. P. Pipe, *Nat. Mater.* **2013**, *12*, 719; c) L. Groenendaal, F. Jonas, D. Freitag, H. Pielartzik, J. R. Reynolds, *Adv. Mater.* **2000**, *12*, 481; d) J. Ouyang, C.-W. Chu, F.-C. Chen, Q. Xu, Y. Yang, *Adv. Funct. Mater.* **2005**, *15*, 203; e) A. Vacca, M. Mascia, S. Rizzardini, S. Corgiolu, S. Palmas, M. Demelas, A. Bonfiglio, P. C. Ricci, *RSC Adv.* **2015**, *5*, 79600.
[20] S. H. Lee, J. S. Sohn, S. B. Kulkarni, U. M. Patil, S. C. Jun, J. H. Kim, *Org. Electron.* **2014**, *15*, 3423.
[21] a) F. Gong, C. Meng, J. He, X. Dong, *Prog. Org. Coat.* **2018**, *121*, 89; b) M. G. Tadesse, C. Loghin, Y. Chen, L. Wang, D. Catalin, V. Nierstrasz, *Smart Mater. Struct.* **2017**, *26*, 065016.
[22] J. Zhou, M. Kimura, *Fiber* **2011**, *67*, 125.
[23] L. Manjakkal, C. G. Núñez, W. Dang, R. Dahiya, *Nano Energy* **2018**, *51*, 604.
[24] X. Wang, A. K. K. Kyaw, C. Yin, F. Wang, Q. Zhu, T. Tang, P. I. Yee, J. Xu, *RSC Adv.* **2018**, *8*, 18334.
[25] a) D. Yoo, J. Kim, J. H. Kim, *Nano Res.* **2014**, *7*, 717; b) F. Zabihi, Y. Xie, S. Gao, M. Eslamian, *Appl. Surf. Sci.* **2015**, *338*, 163.
[26] M. O. P. Kara, M. W. Frey, *J. Appl. Polym. Sci.* **2014**, *131*, 40305.
[27] N. Kumar, R. T. Ginting, J.-W. Kang, *Electrochim. Acta* **2018**, *270*, 37.
[28] Y. Li, G. Ren, Z. Zhang, C. Teng, Y. Wu, X. Lu, Y. Zhu, L. Jiang, *J. Mater. Chem. A* **2016**, *4*, 17324.
[29] A. Choudhury, B. Dey, S. S. Mahapatra, D.-W. Kim, K.-S. Yang, D.-J. Yang, *Nanotechnology.* **2018**, *29*, 165401.
[30] L. Manjakkal, D. Shakthivel, R. Dahiya, *Adv. Mater. Technol.* **2018**, *3*, 1800252.
[31] S. Zhang, N. Pan, *Adv. Energy Mater.* **2015**, *5*, 1401401.
[32] D. Aradilla, P. Gentile, G. Bidan, V. Ruiz, P. Gómez-Romero, T. J. Schubert, H. Sahin, E. Frackowiak, S. Sadki, *Nano Energy* **2014**, *9*, 273.
[33] B. K. Kim, S. Sy, A. Yu, J. Zhang, in *Handbook of Clean Energy Systems*, (Ed: J. Yan), John Wiley & Sons, Ltd., UK **2015**.
[34] A. V. Volkov, K. Wijeratne, E. Mitraka, U. Ail, D. Zhao, K. Tybrandt, J. W. Andreasen, M. Berggren, X. Crispin, I. V. Zozoulenko, *Adv. Funct. Mater.* **2017**, *27*, 1700329.
[35] J. Y. Kim, J. H. Jung, D. E. Lee, J. Joo, *Synth. Met.* **2002**, *126*, 311.
[36] S. Fabiano, N. Sani, J. Kawahara, L. Kergoat, J. Nissa, I. Engquist, X. Crispin, M. Berggren, *Sci. Adv.* **2017**, *3*, e1700345.
[37] S. Lehtimäki, M. Suominen, P. Damlin, S. Tuukkanen, C. Kvarnström, D. Lupo, *ACS Appl. Mater. Interfaces* **2015**, *7*, 22137.
[38] T. Chen, R. Hao, H. Peng, L. Dai, *Angew. Chem., Int. Ed.* **2015**, *54*, 618.
[39] Y. Liu, B. Weng, J. M. Razal, Q. Xu, C. Zhao, Y. Hou, S. Seyedin, R. Jalili, G. G. Wallace, J. Chen, *Sci. Rep.* **2015**, *5*, 17045.
[40] Z. Sun, D. Shu, H. Chen, C. He, S. Tang, J. Zhang, *J. Power Sources* **2012**, *216*, 425.
[41] K. Wang, H. Wu, Y. Meng, Y. Zhang, Z. Wei, *Energy Environ. Sci.* **2012**, *5*, 8384.
[42] C. Zhong, Y. Deng, W. Hu, J. Qiao, L. Zhang, J. Zhang, *Chem. Soc. Rev.* **2015**, *44*, 7484.
[43] D. Zhao, Q. Zhang, W. Chen, X. Yi, S. Liu, Q. Wang, Y. Liu, J. Li, X. Li, H. Yu, *ACS Appl. Mater. Interfaces* **2017**, *9*, 13213.
[44] C. Zhang, T. M. Higgins, S.-H. Park, S. E. O'Brien, D. Long, J. N. Coleman, V. Nicolosi, *Nano Energy* **2016**, *28*, 495.
[45] T. Wakabayashi, M. Katsunuma, K. Kudo, H. Okuzaki, *ACS Appl. Energy Mater.* **2018**, *1*, 2157.
[46] S. B. Singh, T. Kshetri, T. I. Singh, N. H. Kim, J. H. Lee, *Chem. Eng. J.* **2019**, *359*, 197.
[47] D. Yuan, B. Li, J. Cheng, Q. Guan, Z. Wang, W. Ni, C. Li, H. Liu, B. Wang, *J. Mater. Chem. A* **2016**, *4*, 11616.
[48] a) L. Manjakkal, B. Sakthivel, N. Gopalakrishnan, R. Dahiya, *Sens. Actuators, B* **2018**, *263*, 50; b) B. Heng, C. Qing, D. Sun, B. Wang, H. Wang, Y. Tang, *RSC Adv.* **2013**, *3*, 15719.
[49] a) J. Yang, W. Cheng, K. Kalantar-zadeh, *Proc. IEEE* **2019**, *107*, 2168; b) C. Wei, H. Fei, Y. Tian, Y. An, G. Zeng, J. Feng, Y. Qian, *Small* **2019**, *15*, 1903214.